Applied Physics Express 6 (2013) 016503
http://dx.doi.org/10.7567/APEX.6.016503

InGaN Channel High-Electron-Mobility Transistors with InAlGaN Barrier and f_T/f_{max} of 260/220 GHz

Ronghua Wang[1], Guowang Li[1], Golnaz Karbasian[1], Jia Guo[1], Faiza Faria[1], Zongyang Hu[1], Yuanzheng Yue[1], Jai Verma[1], Oleg Laboutin[2], Yu Cao[2], Wayne Johnson[2], Gregory Snider[1], Patrick Fay[1], Debdeep Jena[1], and Huili (Grace) Xing[1]*

[1]*Department of Electrical Engineering, University of Notre Dame, Notre Dame, IN 46556, U.S.A.*
[2]*Kopin Corporation, Taunton, MA 02780, U.S.A.*
E-mail: hxing@nd.edu

Received November 14, 2012; accepted December 5, 2012; published online December 21, 2012

Depletion-mode high-electron-mobility transistors (HEMTs) with an 11 nm quaternary $In_{0.13}Al_{0.83}Ga_{0.04}N$ barrier and a 5 nm $In_{0.05}Ga_{0.95}N$ channel on SiC substrates have been fabricated. The as-processed HEMT structure features a channel electron density of 2.08×10^{13} cm^{-2} and a mobility of 1140 cm^2 V^{-1} s^{-1}. A device with a 50-nm-long T-shaped gate shows a maximum output current density of 2.0 A/mm, a peak extrinsic DC transconductance of 690 mS/mm, and cut-off frequencies f_T/f_{max} of 260/220 GHz at the same bias, representing a record high $\sqrt{f_T \cdot f_{max}}$ of 239 GHz for InGaN channel HEMTs. © 2013 The Japan Society of Applied Physics

Gallium–nitride-based high-electron-mobility transistors (HEMTs) have been intensively studied for radio frequency and power applications. Recently, a current gain cut-off frequency f_T greater than 300 GHz,[1–3] as well as high-performance monolithically-integrated circuits,[4,5] has been demonstrated using both AlN/GaN and InAlN/AlN/GaN heterostructures. To further improve the high-frequency performance, an In(Ga)N channel has been proposed to replace the conventional GaN channel, similar to the established examples of In(Ga)As channel pseudomorphic HEMTs,[6] since InN is predicted to have the highest steady-state peak drift velocity in the GaN material family as a result of its low electron effective mass.[7,8] Though the electron mobility in InGaN is typically lower than that in GaN due to strong alloy scattering, a higher transistor speed may still be expected in ultrascaled HEMTs where mobility plays a less critical role than the electron effective mass. Moreover, the GaN buffer layer naturally acts as a back barrier below the In(Ga)N channel,[9] resulting in improved electron confinement and mitigating short channel effects without compromising the high thermal conductivity offered by the binary III-nitrides. Growth of InGaN channel structures with high mobilities has been challenging due to InGaN instability at high substrate temperatures, as well as strong interface and alloy scattering.[10,11] Recently, we have achieved InGaN channels with a record high mobility μ of 1290 cm^2 V^{-1} s^{-1} and a two-dimensional electron gas (2DEG) density n_s as high as 2.0×10^{13} cm^{-2} by optimizing the InGaN channel thickness, growth temperature, and growth rate in InAlGaN/InGaN/GaN double heterostructures.[12] In terms of device performance, few results have been reported to date: f_T/f_{max} of 65/94 GHz with a 0.18 µm gate length[13] and mitigation of current collapse[14] were reported in $In_{0.10}Ga_{0.90}N$ channel HEMTs. In this work, we present device performance of 50-nm-gate-length InGaN channel HEMTs; f_T/f_{max} of 260/220 GHz was obtained in depletion-mode (D-mode) quaternary barrier $In_{0.13}Al_{0.83}Ga_{0.04}N$ HEMTs with a 5 nm $In_{0.05}Ga_{0.95}N$ channel and regrown ohmic contacts.

The InGaN channel HEMT structure (Fig. 1) consists of an 11 nm $In_{0.13}Al_{0.83}Ga_{0.04}N$ barrier, a 1 nm AlN spacer (total barrier thickness $t_{bar} = 12$ nm), a 5 nm $In_{0.05}Ga_{0.95}N$ channel, and a GaN buffer on SiC substrate, grown by metal organic chemical vapor deposition. Also shown in Fig. 1 is a cross-sectional scanning transmission electron microscopy (STEM) image confirming the existence of the InGaN channel and AlN spacer. A quaternary barrier was employed instead of a ternary $In_{0.17}Al_{0.83}N$ barrier since higher channel mobilities have been consistently observed in the quaternary barrier GaN-channel HEMTs.[15–18] More details on the growth can be found in Ref. 12. Device fabrication started with a molecular beam epitaxy regrowth of a 100 nm n^+ GaN in the ohmic contact region,[19–21] followed by mesa isolation, ohmic metallization (Ti/Au of 20/120 nm), T-gate electrodes defined by electron-beam lithography, metal deposition (Ni/Au of 40/140 nm), and finally a lift-off process. On the as-processed sample, transmission line method measurements revealed a contact resistance R_c of 0.20 Ω mm for the non-alloyed ohmics; room-temperature Hall effect measurements resulted in a sheet resistance R_{sh} of 264 Ω/sq with $n_s = 2.08 \times 10^{13}$ cm^{-2} and $\mu = 1140$ cm^2 V^{-1} s^{-1}. The device has a source/drain (S/D) distance L_{sd} of 1.6 µm, a gate width of 2×25 µm, a gate footprint length of 50 nm, and a mushroom head width of 150 nm. The devices reported here were not passivated.

The band diagrams and charge distributions at equilibrium for several InAlGaN/AlN/(In)GaN heterostructures have been simulated using a self-consistent Shrödinger–Poisson solver[22] and are presented in Fig. 2(a). With the In molar fraction x_{In} in the channel increasing from 0 to 0.10, the back barrier height (i.e., the conduction band offset ΔE_c) increases and the channel quantum well becomes deeper. The presence of the InGaN channel has been confirmed by room-temperature photoluminescence (PL) measurements. The PL peak position was observed to exhibit a gradual redshift from 363 nm (3.41 eV) in the GaN channel HEMT to 421 nm (2.95 eV) in the $In_{0.10}Ga_{0.90}N$ channel HEMT. With an increasing back barrier height, the channel electron confinement is improved, resulting in reduced charge spreading into the GaN buffer. On the other hand, the centroid of the channel charge shifts closer to the AlN interface with increasing In composition, potentially exacerbating the effects of interface scattering in addition to stronger alloy scattering. These effects become more significant in thinner InGaN channels and at higher In compositions. This trend correlates well with our experimental observations shown in

 © 2013 The Japan Society of Applied Physics

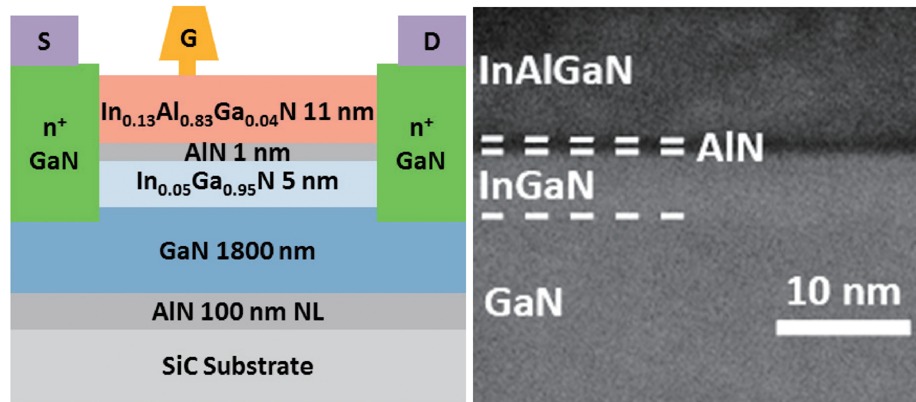

Fig. 1. Schematic cross section of the InAlGaN/AlN/InGaN/GaN HEMT epitaxial layer structure with T-gates and nonalloyed MBE regrown ohmic contacts, and cross-sectional STEM image confirming the InGaN channel thickness.

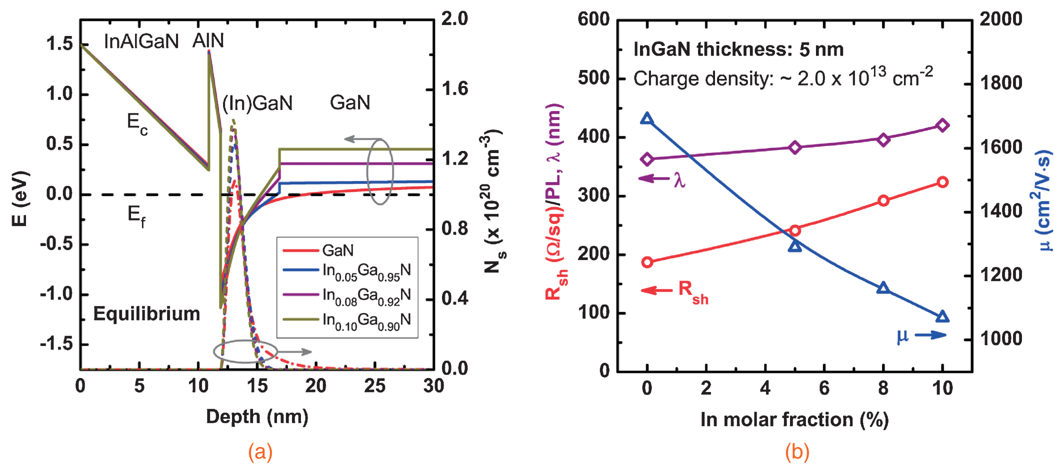

Fig. 2. (a) Simulated band diagram and channel charge distribution in GaN and InGaN channel HEMT structures; (b) room-temperature PL and Hall effect measurement results showing a deeper quantum well and mobility degradation with an increasing In molar fraction in the channel.

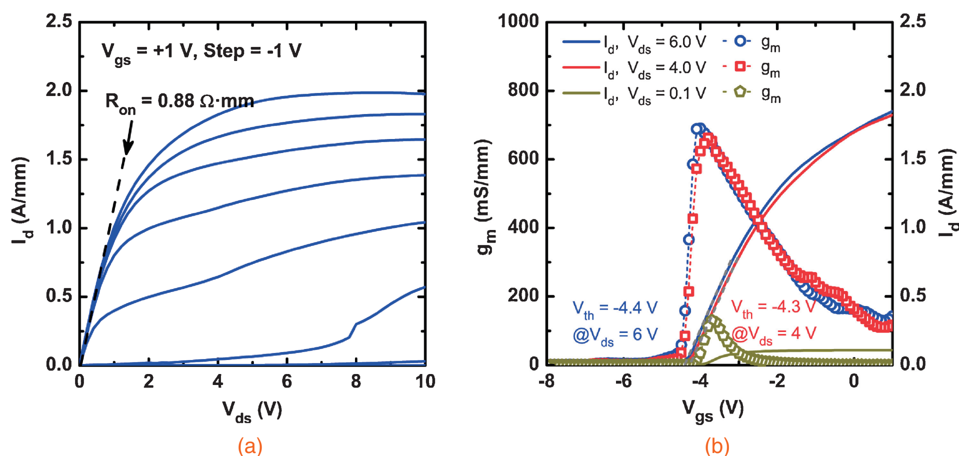

Fig. 3. DC device performance of 50-nm-long $In_{0.05}Ga_{0.95}N$ channel HEMTs: (a) common source family of I–Vs showing $R_{on} = 0.88\,\Omega\,mm$ and $I_{d,max} = 2.0\,A/mm$; (b) linear scale transfer characteristics at $V_{ds} = 0.1$, 4, and 6 V, showing a $g_{m,ext}$ up to 690 mS/mm.

Fig. 2(b), which shows the room-temperature Hall mobility as a function of x_{In} in the $In_xGa_{1-x}N$ channel HEMT structures.[12] Considering that the devices presented here are not deeply scaled in terms of the S/D distance, a moderate In composition of 5% was chosen in the channel as a trade-off to mitigate the impact of a low channel mobility that may lead to a low source injection velocity.

The device common-source family of I–Vs is shown in Fig. 3(a), measured by sweeping V_{ds} from 0 to 10 V and V_{gs} from 1 to −7 V. The maximum output current density $I_{d,max}$ of 2.0 A/mm at $V_{gs} = 1$ V is comparable to that in the conventional quaternary barrier InAlGaN HEMTs with GaN channels[15,17] since the channel charge density and mobility are similar. The device has an on-resistance R_{on} of 0.88

© 2013 The Japan Society of Applied Physics

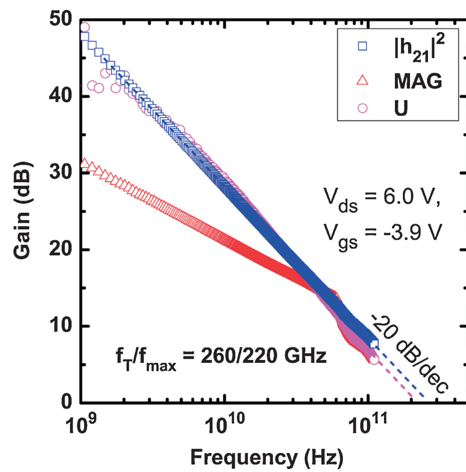

Fig. 4. Small signal current gain and power gain showing $f_T/f_{max} = 260/220$ GHz at $V_{gs} = -3.9$ V and $V_{ds} = 6$ V.

Ω mm extracted from the linear region at $V_{gs} = 1$ V. A three-terminal off-state breakdown voltage V_{br} is measured to be $\sim$15 V at $V_{gs} = -8$ V and $I_d = 1$ mA/mm. The device transfer characteristics are shown in Fig. 3(b), with V_{gs} sweeping from 1 to -8 V at $V_{ds} = 0.1$, 4, and 6 V. A peak extrinsic DC transconductance $g_{m,ext}$ is found to be 660–690 mS/mm near the pinch-off bias condition $V_{gs} \sim -4.0$ V. The threshold voltages V_{th} of -4.0, -4.3, and -4.4 V at $V_{ds} = 0.1$, 4, and 6 V, respectively, are extracted from the linear extrapolation of I_d. In comparison, the threshold voltage values extracted for a GaN channel HEMT with a nominally identical top barrier structure and device geometry are -3.5, -3.9, and -4.0 V at $V_{ds} = 0.1$, 5.6, and 6.6 V, respectively.[18] The more negative V_{th} of the InGaN channel HEMT is likely due to the slightly higher charge in the channel besides the inevitable variations in epitaxy and device fabrication. Meaningful evaluation of short-channel effects requires a detailed, systematic study since these effects are too subtle to base conclusions on a crude comparison across devices. A comprehensive study of the dependence of V_{th} roll-off on In composition, gate length, and bias is planned to address this.

Small signal RF measurements were taken with an Agilent N5250C vector network analyser (VNA) from 100 MHz to 110 GHz. The VNA was calibrated using LRRM off-wafer impedance standards. On-wafer open and short pads were used to de-embed measured S-parameters by subtracting parasitic pad capacitance and inductance.[23] The RF performance of the InGaN channel HEMT near the peak g_m bias conditions ($V_{ds} = 6$ V and $V_{gs} = -3.9$ V) is presented in Fig. 4. After de-embedding, the extrapolation of the current gain $|h_{21}|^2$ with a -20 dB/dec slope yields $f_T = 260$ GHz; the extrapolation of the unilateral power gain U and maximum available power gain MAG gives a similar f_{max} of 220 GHz. The values of f_T/f_{max} before de-embedding were 140/186 GHz. This represents a record value of $\sqrt{f_T \cdot f_{max}} = 239$ GHz achieved in InGaN channel HEMTs. A greater f_{max}/f_T ratio is expected by enlarging the T-gate mushroom head size. Future work includes gate-length and S/D-distance dependent studies to extract the effective electron velocity as well as detailed investigations on short-channel effects in InGaN channel structures.

In conclusion, D-mode $In_{0.13}Al_{0.83}Ga_{0.04}N$ HEMTs with an $In_{0.05}Ga_{0.95}N$ channel were fabricated on SiC substrates with nonalloyed MBE regrown ohmic contacts. T-gate devices with 50-nm-long gate footprints showed a good DC performance of $I_{d,max} = 2.0$ A/mm, $g_{m,ext} = 690$ mS/mm, and a record high f_T/f_{max} of 260/220 GHz in InGaN channel HEMTs.

Acknowledgments This work was supported partly by the Defense Advanced Research Projects Agency (John Albrecht, the NEXT program HR0011-10-C-0015), by the Air Force Office of Scientific Research (Kitt Reinhardt and James Hwang), and by AFRL/MDA (John Blevins, W9113M-10-C-0066).

1) K. Shinohara, D. Regan, A. Corrion, D. Brown, S. Burnham, P. J. Willadsen, I. Alvarado-Rodriguez, M. Cunningham, C. Butler, A. Schmitz, S. Kim, B. Holden, D. Chang, V. Lee, A. Ohoka, P. M. Asbeck, and M. Micovic: IEDM Tech. Dig., 2011, p. 19.1.1.
2) Y. Yue, Z. Hu, J. Guo, B. Sensale-Rodriguez, G. Li, R. Wang, F. Faria, T. Fang, B. Song, X. Gao, S. Guo, T. Kosel, G. Snider, P. Fay, D. Jena, and H. Xing: IEEE Electron Device Lett. **33** (2012) 988.
3) D. S. Lee, B. Lu, M. Azize, X. Gao, S. Guo, D. Kopp, P. Fay, and T. Palacios: IEDM Tech. Dig., 2011, p. 19.2.1.
4) Y. Tang, P. Saunier, R. Wang, A. Ketterson, X. Gao, S. Guo, G. Snider, D. Jena, H. Xing, and P. Fay: IEDM Tech. Dig., 2010, p. 30.4.1.
5) K. Shinohara, D. Regan, A. Corrion, D. Brown, V. Lee, P. M. Asbeck, I. Alvarado-Rodriguez, M. Cunningham, C. Butler, A. Schmitz, S. Kim, B. Holden, D. Chang, A. Margomenos, and M. Micovic: CSICS Tech. Dig., 2012, p. 1.
6) J. A. del Alamo: Nature **479** (2011) 317.
7) B. E. Foutz, S. K. O'Leary, M. S. Shur, and L. F. Eastman: J. Appl. Phys. **85** (1999) 7727.
8) M. Kuzuhara: CS MANTECH Conf. Dig., 2008, p. 2.3.
9) G. Simin, A. Koudymov, H. Fatima, J. Zhang, J. Yang, M. A. Khan, X. Hu, A. Tarakji, R. Gaska, and M. Shur: IEEE Electron Device Lett. **23** (2002) 458.
10) N. Okamoto, K. Hoshino, N. Hara, M. Takikawa, and Y. Arakawa: J. Cryst. Growth **272** (2004) 278.
11) J. Xie, J. H. Leach, X. Ni, M. Wu, R. Shimada, U. Ozgur, and H. Morkoc: Appl. Phys. Lett. **91** (2007) 262102.
12) O. Laboutin, Y. Cao, W. Johnson, R. Wang, G. Li, D. Jena, and H. Xing: Appl. Phys. Lett. **100** (2012) 121909.
13) W. Lanford, V. Kumar, R. Schwindt, A. Kuliev, I. Adesida, A. M. Dabiran, A. M. Wowchak, P. P. Chow, and J.-W. Lee: Electron. Lett. **40** (2004) 771.
14) V. Adivarahan, M. E. Gaevski, M. M. Islam, B. Zhang, Y. Deng, and M. A. Khan: IEEE Trans. Electron Devices **55** (2008) 495.
15) R. Wang, G. Li, O. Laboutin, Y. Cao, W. Johnson, G. Sinder, P. Fay, D. Jena, and H. Xing: IEEE Electron Device Lett. **32** (2011) 1215.
16) R. Wang, G. Li, O. Laboutin, Y. Cao, W. Johnson, G. Sinder, P. Fay, D. Jena, and H. Xing: IEEE Electron Device Lett. **32** (2011) 892.
17) R. Wang, G. Li, J. Verma, T. Zimmermann, Z. Hu, O. Laboutin, Y. Cao, W. Johnson, X. Gao, S. Guo, G. Sinder, P. Fay, D. Jena, and H. Xing: Appl. Phys. Express **4** (2011) 096502.
18) R. Wang, G. Li, G. Karbasian, J. Verma, B. Song, J. Guo, Y. Yue, Z. Hu, O. Laboutin, Y. Cao, W. Johnson, G. Snider, P. Fay, D. Jena, and H. Xing: Abstr. Int. Workshop Nitride Semiconductors, 2012, p. ED7-2.
19) J. Guo, Y. Cao, C. Lian, T. Zimmermann, G. Li, J. Verma, X. Gao, S. Guo, M. Wistey, D. Jena, and H. Xing: Phys. Status Solidi A **208** (2011) 1617.
20) J. Guo, G. Li, F. Faria, Y. Cao, R. Wang, J. Verma, X. Gao, S. Guo, E. Beam, A. Ketterson, M. Schuette, P. Saunier, M. Wistey, D. Jena, and H. Xing: IEEE Electron Device Lett. **33** (2012) 525.
21) F. Afroz Faria, J. Guo, P. Zhao, G. Li, P. K. Kandaswamy, M. Wistey, H. G. Xing, and D. Jena: Appl. Phys. Lett. **101** (2012) 032109.
22) 1D Poisson software [http://www.nd.edu/~gsnider].
23) M. C. A. M. Koolen, J. A. M. Geelen, and M. P. J. G. Versleijen: Proc. BCTM, 1991, p. 188.

 © 2013 The Japan Society of Applied Physics